




Cite this: *Phys. Chem. Chem. Phys.*,  
2023, 25, 28196

# An effective model for sodium insertion in hard carbons

Huy Sy Nguyen \*<sup>ab</sup> and Arnulf Latz <sup>abc</sup>

Sodium ion batteries (NIBs) are a potential alternative to Lithium ion batteries (LIBs) because of their lower cost and greater availability. As anodes, hard carbons (HCs) seem to be the most promising candidates for NIBs. Previous numerical theoretical research studies have focussed on the general conditions for Na insertion in HCs, while experiments have shown that the properties of Na insertion in HCs depend strongly on specific material properties of HCs. Our target is building an effective model based on experimental data and the volume expansion phenomenon as a base for constructing chemical potentials and free energies efficiently as the starting point for continuum modeling of intercalation in HCs. In our effective model, HC is treated implicitly, while Na is simulated in a confined space, created by the HC. To reproduce the complex intercalation behavior of Na, different intercalation sites at different energy levels must be introduced. The results show good agreement with the experimental data and clarify the contribution of different Na insertion sites and the exchange between different sites of Na to the open circuit voltage as well as their contribution to the reversible and irreversible capacity of Na in HCs.

Received 6th July 2023,  
Accepted 20th September 2023

DOI: 10.1039/d3cp03186a

rsc.li/pccp

## 1. Introduction

Lithium ion batteries (LIBs) have many applications in commercial electronic devices<sup>1</sup> and vehicles, energy storage, military<sup>2</sup> and others, due to their high energy density and low self-discharge.<sup>2</sup> However, limited Li resources on the Earth lead to high costs of LIBs<sup>3,4</sup> while the demand for energy storage capacity continues to increase. Sodium ion batteries (NIBs) are a potential alternative to LIBs because NIBs have similar electrochemical properties to LIBs but at a much lower cost since Na is an Earth abundant material.<sup>3,4</sup> Unfortunately, graphite, the traditional anode of LIBs<sup>5–9</sup> is not suitable for NIBs<sup>10</sup> because of low capacity<sup>3</sup> and high volume expansion.<sup>11</sup> Among several anodes for NIBs, such as MXenes,<sup>3</sup> C<sub>6</sub>B<sub>4</sub>,<sup>12</sup> blue – phosphorene,<sup>13</sup> and 1H-BeP<sub>2</sub>,<sup>14</sup> hard carbon (HC) is a promising anode for NIBs because of stable cycling, large specific capacity,<sup>15</sup> and low-cost biomass product precursors.<sup>15,16</sup>

Besides experimental studies,<sup>17–20</sup> there are several theoretical investigations of Na-insertion in HCs. At the atomic level, the simplest models use density functional theory (DFT) to calculate the adsorption energy of Na in a graphite layer with some heteroatoms.<sup>21–23</sup> DFT results can be combined with

operando Raman spectra to study the mechanism of Na insertion in HCs.<sup>24,25</sup> For further calculations, Cai *et al.* studied the insertion of Na between two graphitic layers<sup>26</sup> and Youn *et al.* suggested the crystalline phase of Na inside HCs at high capacity.<sup>27</sup>

While DFT studies reveal the separate atomistic mechanisms of Na insertion in HCs, continuum models are used for quantitative simulation of Na insertion in HCs on larger scales. Previous continuum models for Na insertion in HCs used 2-level models describing intercalation + pore filling<sup>28</sup> or 3-level models for capturing adsorption, intercalation, and pore filling.<sup>29</sup> However, a complete understanding of Na insertion in HCs is more complicated than this. Reddy *et al.*<sup>24</sup> suggested 4 types of Na insertion in HCs, including adsorption of Na on the surface of the graphitic layer, on defect sites of HCs, intercalation of Na in graphitic sheets and inter-pore Na, filling the pores of HCs. Both the 2-level model and the 3-level model ignored the defect Na, but the defect Na should not be neglected for 2 reasons: on the one hand, the heteroatom defects always appear in HCs,<sup>23</sup> and on the other hand, some experimental studies use heteroatom doping defects to increase the capacity.<sup>30–33</sup>

Moreover, these models investigated the generic case of Na insertion in HCs, while experiments proved that the properties of Na insertion in HCs depends strongly on the specific material properties of HCs.<sup>34–37</sup> Bommier *et al.* predicted Na capacity based on the pore volume and surface area of HCs; however, the mechanism of Na insertion in HCs is not considered in their study.<sup>38</sup> The picture is more complicated when

<sup>a</sup> Department of Electrochemistry, University of Ulm, Albert-Einstein-Allee 47, 89081 Ulm, Germany. E-mail: huy.nguyen@dlr.de, Arnulf.Latz@dlr.de

<sup>b</sup> Institute of Engineering Thermodynamics, German Aerospace Center (DLR), Wilhelm-Runge-Str. 10, 89081 Ulm, Germany

<sup>c</sup> Helmholtz Institute Ulm (HIU), Helmholtzstr. 11, 89081, Ulm, Germany



the HC structure can change during the charge/discharge process: Sauerteig *et al.* observed that the volume of HC expanded by up to 10% in the first charge/discharge cycle and 5% in the later cycles.<sup>39</sup>

Besides the insertion mechanism, the reversible and irreversible capacity are also important factors for battery applications. Olsson *et al.* calculated the adsorption energy of Na atoms at the defect points to study the irreversible contribution of defect Na.<sup>22</sup> Jensen *et al.* studied migration barriers to estimate the mobility of Na atoms in HCs.<sup>40</sup> However, these studies are qualitative and do not provide the full picture of reversible and irreversible effects for each type of Na in HCs.

In this work, we develop an effective model to investigate the Na insertion into HCs dependent on structural features of hard carbon and the energetic properties of different insertion mechanisms. The purpose of our model is to provide a frame in which known experimental materials data and results from *ab initio* simulations can be used to relate the SOC to the internal states of the inserted Na ions and to create a base for future continuum simulations, in which the OCV and the distribution of Na over internal states also in non-equilibrium (charge and discharge) situations is needed. Our effective model is therefore a crucial step for the development of a multi-scale approach for Na batteries based on materials data and *ab initio* simulations. This model is based on the experimental data and includes volume expansion to cover all aspects of Na insertion in HCs. In this model, Na atoms are simulated in the confined space created by HCs, where the full energetics of the different insertion mechanisms are covered.

This paper is arranged as follows. The effective model and the different energy states of Na in HCs are described in detail in Section 2. The results are shown and compared with experiments in Section 3. The mechanism and interchange between different states of Na are also clarified in this section. Finally, the conclusion is provided in Section 4.

## 2. Model

### 2.1 Effective model

**2.1.1 Thermodynamic model.** Considering a simplified scheme for a half cell as in Fig. 1 with Na metals as a counter electrode for hard carbons ionically coupled through an

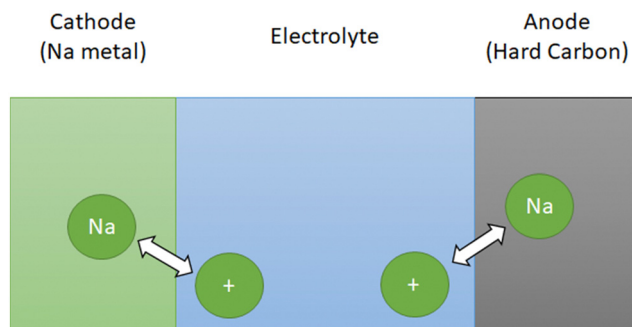
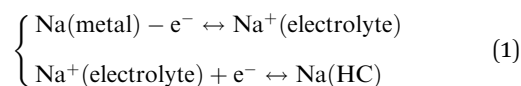


Fig. 1 Battery system.

electrolyte, the fundamental reaction scheme in this system is



Eqn (1) assumes that in equilibrium, the concentration of  $\text{Na}^+$  in the electrolyte is constant and the total sum of Na atoms in the cathode and anode is also constant. For our thermodynamic model, we only need the transfer of  $\text{Na}^+$  ions from a reservoir to the hard carbon electrode, where the total amount of  $\text{Na}^+$  remains constant. The thermodynamic model introduced in this paper studies the equilibrium capacity of Na atoms in HC at different voltages. Other properties such as transport<sup>41</sup> or the diffusion pathway, electrochemical double layer,<sup>42</sup> and solid electrolyte interface (SEI)<sup>43</sup> will be investigated in future papers.

**2.1.2 Effective model.** In the thermodynamic model, the Na metal was replaced (Fig. 2) with an *NVT* ensemble with a fixed number of neutral Na-atoms distributed in a reservoir (outer zone) and the hard carbon (HC) (see Fig. 3). The reservoir and the HC are in equilibrium. The chemical potential of the neutral Na in the reservoir and the neutral inserted Na are the same. The voltage of the cell is the difference in the chemical potential of the inserted Na in HCs and the chemical potential of Na in the neutral Na metal. Instead of tuning the electric potential, we tune the chemical potential of the Na in the reservoir to change the SOC of the HC through the equilibrium constraint

$$\mu_{\text{out}} = \mu_{\text{HC}} \quad (2)$$

This is effectively the same as tuning the potential difference between the Na metal and HC. Thus, our effective model, Fig. 3, consists of 2 different zones: HC and outer zone with the chemical potential:  $\mu_{\text{HC}}$  and  $\mu_{\text{out}}$ , respectively. The equilibrium constraint requires the chemical potentials of both zones to be the same, eqn (2).

In our simulation, it is convenient to use the energy  $\varepsilon_{\text{out}}$  and  $\varepsilon_{\text{HC}}$  for the outer zone and HC, respectively. The relationship

Cathode  
(Na metal)      Anode  
(Hard Carbon)

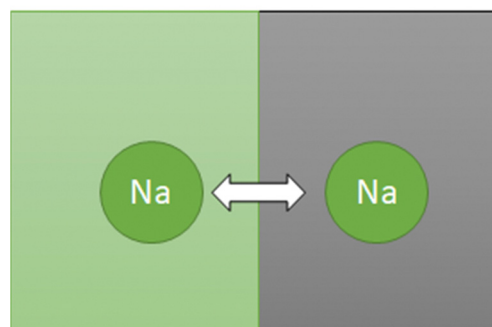


Fig. 2 Thermodynamic model.



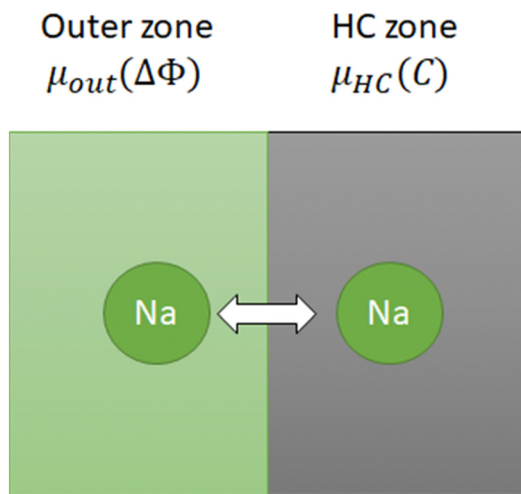


Fig. 3 Effective model.

between the energy and chemical potential is  $\mu_{out} = \partial \varepsilon_{out} / \partial N_{out}$  and  $\mu_{HC} = \partial \mu_{HC} / \partial N_{HC}$ .

## 2.2 Model hard carbon

To model specific HC materials, we use property data obtained from their characterization, including the length of the graphitic layer  $L_a$ , the layer thickness  $L_c$ , the pore volume  $V_p$ , and the swelling coefficient  $K_{SW}$ . The  $L_a$ ,  $L_c$ , and  $V_p$  values are used to model the unit cell of HC while  $K_{SW}$  is used to describe the interaction between Na and HC.

**2.2.1 Structure of hard carbons.** There are several structures of HCs.<sup>29</sup> Recent research studies have used the model 'house of cards' proposed by Dann.<sup>28,45,46</sup> However, in our effective model, the random crystal structure proposed by Franklin is chosen because it is simply to model and demonstrate different types of Na insertion in HCs.

**2.2.2 Unit cell of HCs.** In our effective model, the 'unit cell of HCs' includes a pore, confined by many graphitic boundary layers. The different graphitic sheets are parallel and separated from each other by a distance  $d_l$ . All layers have the same length  $L_a$ ; while the number of layers depends on the ratio of the average thickness of the graphitic domain  $L_{c0}$  and the distance between layers  $d_l$ . The pore volume in the experiment  $V_p$  is equal to the volume of the cylindrical pore.

In this simulation, the number of boundary layers adjacent to a pore is set to 3 for simplicity.  $L_a$  and  $L_{c0}$  are obtained from Raman spectra and  $V_p$  is obtained from BET.<sup>37</sup> The figure and parameters of the unit cell are shown in Table 1 and Fig. 4.

Table 1 Parameters of a unit cell of hard carbons<sup>37</sup>

Parameters, unit	Value
$L_a$ , nm	2.06
$L_{c0}$ , nm	1.10
$V_p$ , cm <sup>3</sup> g <sup>-1</sup>	0.10

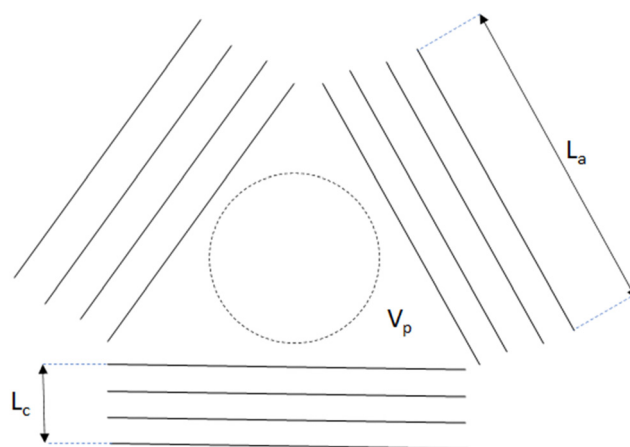


Fig. 4 Unit cell of hard carbon.

**2.2.3 The expansion of hard carbons.** The graphitic layer thickness increases during the charge-discharge process. This swelling is linear with the total capacity:<sup>39</sup>

$$L_c = L_{c0}[1 + A_{SW}(C)] \quad (3)$$

In the effective model, the relationship between layer distance  $d_l$  and layer thickness  $L_c$  is

$$d_l = L_c / (n - 1) \quad (4)$$

where  $n$  is the number of graphitic layers in each side of the boundary layer.

The distance between 2 graphitic layers  $d_l$  is in the range of 0.309–0.404 nm.<sup>23</sup> In the effective model,  $n$  is set to 4 and the layer distance  $d_l$  is about:

$$d_l = L_c / (n - 1) \approx L_{c0} / 3 \approx 0.367 \text{ nm} \quad (5)$$

## 2.3 Model Na

**2.3.1 Types of Na.** In our effective model, (Fig. 5) 5 types of Na are defined:

- Outer Na: in the outer zone.
- Interpore Na: inside the pore.
- Interlayer Na: in between 2 graphitic layers.
- Adsorption Na: close to a graphitic layer.
- Defect Na: close to defect points in the graphitic layer.

**2.3.2 Energy levels of Na.** The energy between Na and HC is a function of Na concentration. In this work, we use the

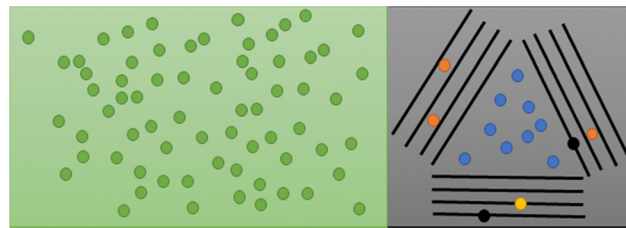


Fig. 5 Schematic of effective model: outer Na (green) in the outer zone (light green); interpore Na (blue), interlayer Na (orange), adsorption Na (black) and defect Na (yellow) in HC zone (grey).



relationship between the energy and Na concentration of each type of Na obtained from mechanisms,<sup>24</sup> DFT calculations,<sup>21,23</sup> Bragg-Williams model,<sup>28</sup> and experiments.<sup>26</sup> However, the energy parameters should be changed because they depend strongly on each type of ion insertion and the specific HC. These energy parameters in this work are applied for Na<sup>+</sup>, but the effective model can be extended to different ions such as K<sup>+</sup>, Mg<sup>2+</sup>, and Zn<sup>2+</sup> with different energy parameters.

*a. The total energy.* The total energy in the system is

$$E_{\text{tot}} = N_{\text{out}}\varepsilon_{\text{out}} + N_{\text{p}}\varepsilon_{\text{p}} + N_{\text{l}}\varepsilon_{\text{l}} + N_{\text{d}}\varepsilon_{\text{d}} + N_{\text{f}}\varepsilon_{\text{f}} \quad (6)$$

where  $N_{\text{out}}$ ,  $N_{\text{p}}$ ,  $N_{\text{l}}$ ,  $N_{\text{d}}$ , and  $N_{\text{f}}$  are the number of Na atoms in the different energy states: outer, intercore, interlayer, adsorption, and defect, respectively.

$\varepsilon_{\text{out}}$ ,  $\varepsilon_{\text{p}}$ ,  $\varepsilon_{\text{l}}$ ,  $\varepsilon_{\text{d}}$ , and  $\varepsilon_{\text{f}}$  are the energies per Na atom in the corresponding states. In the effective model, the total Na atoms,  $N_{\text{tot}}$  is kept as constant, but the number of Na atoms in each energy state can fluctuate, which means Na can switch between states.

$$N_{\text{out}} + N_{\text{p}} + N_{\text{l}} + N_{\text{d}} + N_{\text{f}} = N_{\text{tot}} = \text{constant} \quad (7)$$

According to the literature,<sup>24</sup> we have

$$\varepsilon_{\text{d}}, \varepsilon_{\text{f}} < \varepsilon_{\text{l}} < \varepsilon_{\text{p}} \quad (8)$$

In the effective model, the Na atoms are modelled as hard spheres with radius  $r_{\text{Na}} = 0.106$  nm.<sup>47</sup> Using the mean-field theory,<sup>28</sup> the energy per Na atom in different states depends on the number of Na atoms in each other state.

*b. The energy in the outer state  $\varepsilon_{\text{out}}$ .* In the effective model, all atoms in the outer state have the same energy  $\varepsilon_{\text{out}}$ . The energy level in the outer state is regulating the state of charge (SOC) of the electrode *i.e.*, for  $\varepsilon_{\text{out}} < \varepsilon_{\text{d}}$ ,  $\varepsilon_{\text{f}} < \varepsilon_{\text{l}} < \varepsilon_{\text{p}}$  all Na are in the outer zone. For  $\varepsilon_{\text{d}}, \varepsilon_{\text{f}} < \varepsilon_{\text{l}} < \varepsilon_{\text{p}} < \varepsilon_{\text{out}}$ , all Na are in HC zone. By varying  $\varepsilon_{\text{out}}$ , the SOC is varying smoothly from zero to one.

*c. Defect energy  $\varepsilon_{\text{f}}$ .* Experimental XPS measurements identify commonly a 4% oxygen defect in HC.<sup>23</sup> There are 4 possible types of defects: single substitutional oxygen defect ( $\text{O}_{\text{C}}$ ), single substitutional oxygen defect and carbon vacancy ( $\text{O}_{\text{C}}\text{V}_{\text{C}}$ ), double substitutional oxygen defect ( $2\text{O}_{\text{C}}$ ) and triple substitutional oxygen defect ( $3\text{O}_{\text{C}}$ ).  $\text{O}_{\text{C}}$  and  $2\text{O}_{\text{C}}$  are purely substitutional in nature<sup>23</sup> and more common than others.<sup>22</sup>

Based on these results, we set the number of defect points to 4% of the number of the total carbon atom,  $n_{\text{Carbon}}$  in the system. The coordinates of the defect points are fixed. Every defect point of  $\text{O}_{\text{C}}$  has the same energy  $\varepsilon_{\text{f1}}$  and every defect point of  $2\text{O}_{\text{C}}$  has the same energy  $\varepsilon_{\text{f2}}$ .

$$n_{\text{O}_{\text{C}}} + n_{2\text{O}_{\text{C}}} + n_{\text{O}_{\text{C}}\text{V}_{\text{C}}} + n_{3\text{O}_{\text{C}}} \approx n_{\text{O}_{\text{C}}} + n_{2\text{O}_{\text{C}}} = 0.04n_{\text{Carbon}} \quad (9)$$

The last term on the right-hand side of eqn (6) can therefore be rewritten as

$$\begin{cases} N_{\text{f}}\varepsilon_{\text{f}} = N_{\text{f1}}\varepsilon_{\text{f1}} + N_{\text{f2}}\varepsilon_{\text{f2}} \\ N_{\text{f}} = N_{\text{f1}} + N_{\text{f2}} \end{cases} \quad (10)$$

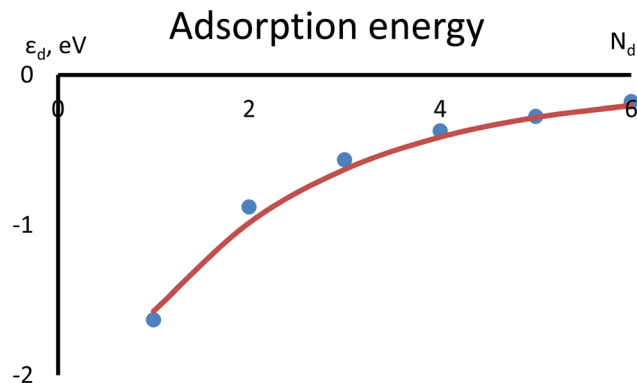


Fig. 6 Adsorption energy as a function of the number of Na atoms. Dots and lines are obtained from DFT<sup>21</sup> and eqn (11), respectively.

where  $N_{\text{f1}}$  and  $N_{\text{f2}}$  are the number of Na atoms adsorbing on defect points  $\text{O}_{\text{C}}$  and  $2\text{O}_{\text{C}}$ , respectively.

*d. Adsorption energy  $\varepsilon_{\text{d}}$ .* In DFT calculations,<sup>21</sup> the adsorption energy of Na adsorption  $\varepsilon_{\text{d}}$  is a function of Na concentration. In this work, we use the fitted equation, which  $\varepsilon_{\text{d}}$  can be approximated as:

$$\varepsilon_{\text{d}} = \varepsilon_{\text{d}}^0 + a_{\text{d}} \exp\left(-\frac{N_{\text{d}}}{b_{\text{d}}}\right) \quad (11)$$

If the DFT results can be extrapolated to zero and large occupation:  $N_{\text{d}} = 0$  and ( $N_{\text{d}} \gg b_{\text{d}}$ ), respectively,  $a_{\text{d}}$  can be interpreted as the energy difference between a Na atom at the adsorption site and in vacuum.  $\varepsilon_{\text{d}}^0$  would be the energy between a fully occupied interface and vacuum.

The DFT data and fit with eqn (11) are shown in Fig. 6.

In our effective model, we distinguish between Na adsorbed on the outer graphitic layer and Na inserted between the graphitic layer ("interlayer Na"). The energy scale  $a_{\text{d}}$  and the particle scale  $b_{\text{d}}$  are adjusted so that the interlayer position becomes energetically preferable for  $N_{\text{d}} > b_{\text{d}}$ , if the number  $N_{\text{d}}$  of adsorbed Na atoms are exceeding  $b_{\text{d}}$ , Na preferentially occupy interlayer positions.

*e. Interlayer energy  $\varepsilon_{\text{l}}$ .* The value of  $\varepsilon_{\text{l}}$  not only depends on the number of interlayer Na,  $N_{\text{l}}$ <sup>28</sup> but also on the distance between 2 graphitic layers,  $d_{\text{l}}$ .<sup>26</sup> The value  $\varepsilon_{\text{l}}$  can be expressed as:

$$\varepsilon_{\text{l}} = \varepsilon_{\text{l}}^0 + l_1(d_{\text{l}}) + l_2(x_{\text{l}}) \quad (12)$$

where  $d_{\text{l}}$  is the distance between 2 graphitic layers in HC. At the value  $d_{\text{l}} = 0.34$  nm, the distance between 2 graphitic layers in graphite, the function  $l_1(d_{\text{l}})$  is very high which might explain why Na is difficult to intercalate into graphite.<sup>26</sup> In our model,  $l_1(d_{\text{l}})$  can be expressed as:

$$l_1(d_{\text{l}}) = \frac{a_{\text{l}}}{\frac{d_{\text{l}}}{d_{\text{min}}} - 1} \quad (13)$$

where  $a_{\text{l}} > 0$  is the energy scale of the interlayer energy as a function of  $d_{\text{l}}$ , and  $d_{\text{min}}$  is the minimum distance between 2 graphitic layers where Na can intercalate.



The function  $l_1(d_1)$  diverges when  $d_1 = d_{\min}$ , which means the layer spacing is too narrow and Na cannot intercalate.

The  $d_1$  value is calculated from the graphitic layer thickness:

$$d_l = \frac{L_c}{3} = \frac{L_{c0}[1 + \Delta_{sw}(C)]}{3} \quad (14)$$

where  $L_{c0} = 1.1$  nm is obtained from experiment.<sup>37</sup>  $\Delta_{sw}$  is the swelling during the charge/discharge process and varies linearly with the capacity<sup>39</sup>

$$\Delta_{sw}(C) = K_{sw} \frac{N_{sw}}{N_{sw}^{\max}} \quad (15)$$

where  $K_{sw}$  is the swelling coefficient. Experiments show that the layer thickness expands up to 10% in the 1st cycle and 5% in later cycles.<sup>26</sup> In simulations,  $K_{sw}$  is set as 0.1 and 0.05 for the 1st and 10th cycles, respectively.

$N_{sw}$  is all Na causing layer thickness swelling. In Fig. 6, they include defect Na, adsorbed Na and interlayer Na.

$$N_{sw} = N_f + N_d + N_l \quad (16)$$

$N_{sw}^{\max}$  is the maximum of Na causing layer thickness swelling.

$$N_{sw}^{\max} = N_f^{\max} + N_d^{\max} + N_l^{\max} \quad (17)$$

The function  $l_2(x_1)$  is a polynomial function of  $x_1$ , depending on  $N_l$ :

$$x_1 = \frac{N_l}{(N_{\text{Carbon}}/24)} \quad (18)$$

According to Reddy *et al.*, Na will intercalate until the structure is between  $\text{NaC}_{24}$  and  $\text{NaC}_{12}$ .<sup>24</sup> The value of  $x_1$  should be in the range:  $1 \leq x_1 \leq 2$ .

*f. Interpore energy  $\varepsilon_p$ .* According to the literature, the properties of  $\varepsilon_p$  are complicated compared with those of  $\varepsilon_l$ :

- In DFT calculations,<sup>26</sup> the insertion energy of Na into the confined space between graphitic layers decreases with the distance between Na and the nearest graphitic layer. Note that the pore radius,  $r_p$  is larger than the thickness of the layer  $d_l$  which implies  $\varepsilon_p < \varepsilon_l$ .

- Interpretations from experiments<sup>24</sup> suggest that Na fills the pore after intercalating between graphitic layers which implies  $\varepsilon_p > \varepsilon_l$ .

To combine these statements,  $\varepsilon_p$  is expressed as follows:

$$\varepsilon_p = p_1(r_p)p_2(N_p) + p_3(x_p) \quad (19)$$

where  $\varepsilon_p$  quantifies the probability of insertion of the first Na into the pore. It has the same form as  $l_1(d_1)$  and varies with the pore radius  $r_p$  as

$$p_1(r_p) = \frac{a_l}{\frac{2r_p}{b_l d_{\text{graphite}}} - 1} \quad (20)$$

$p_2(N_p)$  quantifies the probability of insertion the other Na into the pore after the first Na insertion.

$$p_2(N_p) = \frac{1 + a_p N_p}{1 + N_p} \quad (21)$$

Due to the large change of  $p_2$  upon varying  $N_p$ , Na will intercalate into graphitic layers before filling the pore.

$p_3(x_p)$  mimics the interaction between Na in the pore. In our effective model, this term is approximated using the pore occupation fraction  $x_p = N_p/N_p^{\max}$

$$p_3(x_p) = b_p x_p \quad (22)$$

**2.3.3 The reversible and irreversible capacities.** The reversible and irreversible capacities of Na in HC are estimated by comparing the OCV results of the 1st and later cycles. Upon cycling, some of the inserted Na are trapped inside HCs leading to an irreversible capacity loss. In this paper, we approximate the irreversible capacity loss by comparing the number of Na ions participating in cycling at the 1st and 10th cycle. For convenience, all input energy parameters are summarized in Table 2.

## 2.4 Simulation

Monte Carlo NVT simulation is applied for simulating the effective model. As mentioned in Section 2.3.1, the total volume  $V$  contains the outer zone and the HC zone, while the total number of Na in both the outer zone and the HC zone,

Table 2 Parameters of 1st and 10th cycles

Type	Parameters	Equation	1st cycle	10th cycle
Outer Na	$\varepsilon_{\text{out}}$	(6)	$\varepsilon_{\text{out}} = -3.0$ to $0.0$ eV	
Defect Na	$\varepsilon_{f1}$	(10)	$-2.2$ eV	$0.0$ eV
	$\varepsilon_{f2}$	(10)	$0.0$ eV	$0.0$ eV
Adsorption Na	$\varepsilon_d^0$	(11)	$0.0$ eV	$0.0$ eV
	$a_d$	(11)	$-3.0$ eV	$-3.0$ eV
Interlayer Na	$\varepsilon_l^0$	(12)	$-1.3$ eV	$-1.3$ eV
	$l_2(x_1)$	(12)	$l_2(x_1) = c_1 x_1 + e_1 x_1^2 + f_1 x_1^3$ $c_1 = 0.3$ eV, $e_1 = -0.34$ eV $f_1 = 0.18$ eV	$l_2(x_1) = g_1 x_1^{0.5}$ $g_1 = 0.74$ eV
	$a_l$	(13)	$0.01$ eV	$0.01$ eV
	$d_{\min}$	(13)	$0.3383$ nm	$0.3383$ nm
	$L_{c0}$	(14)	$1.1$ nm	$1.155$ nm
	$K_{sw}$	(15)	$0.1$	$0.05$
Interpore Na	$a_p$	(21)	$0.2$	$0.13$
	$b_p$	(22)	$0.1$ eV	$0.06$ eV





$N_{\text{tot}} = 648$ , is also kept constant, while the number Na in each state of Na will change. The temperature is chosen at  $T = 25^\circ\text{C}$ . The outer potential energy  $\varepsilon_{\text{out}}$  is varied to find the equilibrium condition of Na. The Monte Carlo simulation is run with Markov chain<sup>48,49</sup> including  $10^7$  steps. Each step loops over all 648 Na atoms. In this work, we do not compare with *ab initio* NVT simulation. Alternatively, we compare directly with experiments.

The cell voltage is calculated as:<sup>44</sup>

$$e\varphi = \varepsilon^0 - \mu = \varepsilon^0 - (\mu^{\text{id}} + \mu^{\text{ex}}) = \varepsilon^0 - \left\{ k_B T \ln \frac{N_{\text{HC}}}{N_{\text{HC}}^{\text{max}}} + \mu^{\text{ex}} \right\} \quad (23)$$

where:

$\varepsilon^0$  (eV) is the interaction between Na and the counter electrode that shifts the voltage scale,  $k_B = 8.61733 \times 10^{-5} \text{ eV K}^{-1}$  is the Boltzmann constant,  $T = 25^\circ\text{C} = 298.15 \text{ K}$ ,  $N_{\text{HC}} = N_p + N_l + N_d + N_f$  is the total Na in HC,  $N_{\text{HC}}^{\text{max}}$  is the maximum Na in HC, and  $\mu^{\text{ex}}$  (eV) is the excess chemical potential obtained from Widom's insertion method.<sup>48,49</sup> In our effective model, ions are only inserted in HCs, while the total number of ions in the outer zone and HCs are constant, eqn (7).

## 3. Results and discussion

### 3.1 Comparison with experiment

In Fig. 7, the OCV results of the 1st and 10th cycles are compared with the experiment. The capacities determined from simulation in the 1st and 10th cycles are  $537 \text{ mA h g}^{-1}$  and  $325 \text{ mA h g}^{-1}$ , respectively, compared with  $507 \text{ mA h g}^{-1}$  and  $322 \text{ mA h g}^{-1}$  from experiments. This excellent agreement with our effective model based on specific material properties motivates us to study in detail the insertion mechanism and the cause of the reversible – irreversible capacity of Na insertion in HC.

### 3.2 Mechanism of Na insertion in HCs

The order of the different mechanisms of Na insertion in HC is illustrated in Fig. 8. In the 1st cycle, at first, Na adsorbs on defect  $\text{O}_\text{C}$  of HC. At a capacity of  $C = 10 \text{ mA h g}^{-1}$ , Na adsorbs on the surface of graphitic layers. The adsorption Na has a dip in this zone from  $C = 25 \text{ mA h g}^{-1}$  to  $C = 210 \text{ mA h g}^{-1}$  due to the interchange between adsorption Na and interlayer Na, Na atoms intercalate until the structure  $\text{NaC}_{15.3}$  is formed ( $x_1 \sim 1.57$ ). This value is close to other DFT results for  $\text{NaC}_{16}$ .<sup>50–52</sup> Finally, Na can only be filled in the pore of HC from a capacity of  $C > 210 \text{ mA h g}^{-1}$ . Na is not adsorbed on  $2\text{O}_\text{C}$  defects. The mechanism of Na insertion in HCs in the 10th cycle is similar to that in the 1st cycle. However, there are no insertions to defect  $\text{O}_\text{C}$  sites in the 10th cycle, which means that all adsorption to defect sites  $\text{O}_\text{C}$  are irreversible.

### 3.3 The relationship between the upper limit of adsorption Na $b_d$ and the energy in the outer state $\varepsilon_{\text{out}}$

In simulation, we vary  $\varepsilon_{\text{out}}$  and change  $b_d$  to fit with experiments. Interestingly, we found a linear relationship between  $\varepsilon_{\text{out}}$  and  $b_d$ , Fig. 9. The value of  $b_d$  increases with  $\varepsilon_{\text{out}}$  and we can estimate  $b_d$  from  $\varepsilon_{\text{out}}$ . Moreover, the value of  $b_d$  in the 1st cycle is much higher than the 10th cycle, which means that most of adsorption Na are trapped inside HC during the charge – discharge process. This will be discussed further in the next section.

### 3.4 Approximating reversible and irreversible capacities

As shown in Fig. 10, Na atoms adsorb irreversibly on defect points. The degree of reversibility of Na at adsorption sites is also relatively small because their mobility is restricted by interlayer Na, Fig. 5. The fraction of reversible capacity of interlayer Na is very high, about 80%, due to the weak interaction between graphitic layers and inserted Na, whereas the adsorption energy of Na on graphitic layers is relatively large. Therefore, interlayer Na can move freely as does the interlayer Na. This can be inferred from the comparable reversibility of interlayer Na and interlayer Na. The larger reversibility of the

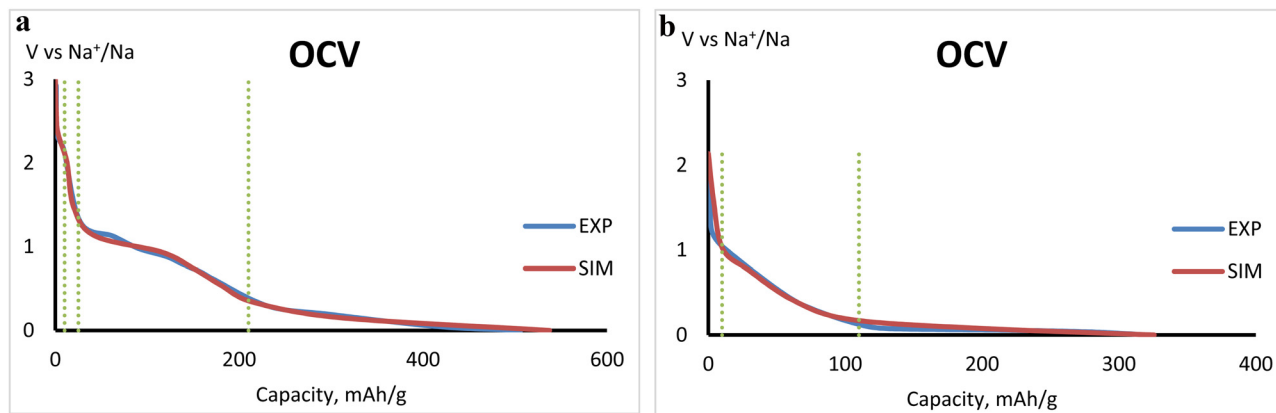


Fig. 7 (a) The OCV results of the 1st cycle obtained from experiment (blue line) and simulation (red line). (b) The OCV results of the 10th cycle obtained from experiment (blue line) and simulation (red line).



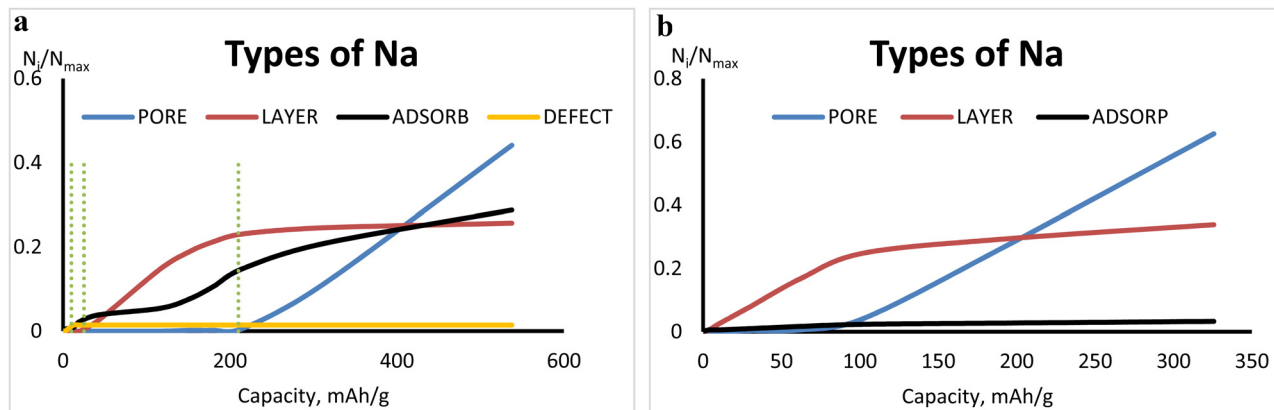


Fig. 8 (a) Proportion of types of Na in HC of the 1st cycle. The inter pore Na, interlayer Na, adsorption Na and defect Na are the blue, red, black, and orange lines, respectively. (b) Proportion of types of Na of the 10th cycle. The inter pore Na, interlayer Na, and adsorption Na are the blue, red, and black lines, respectively.

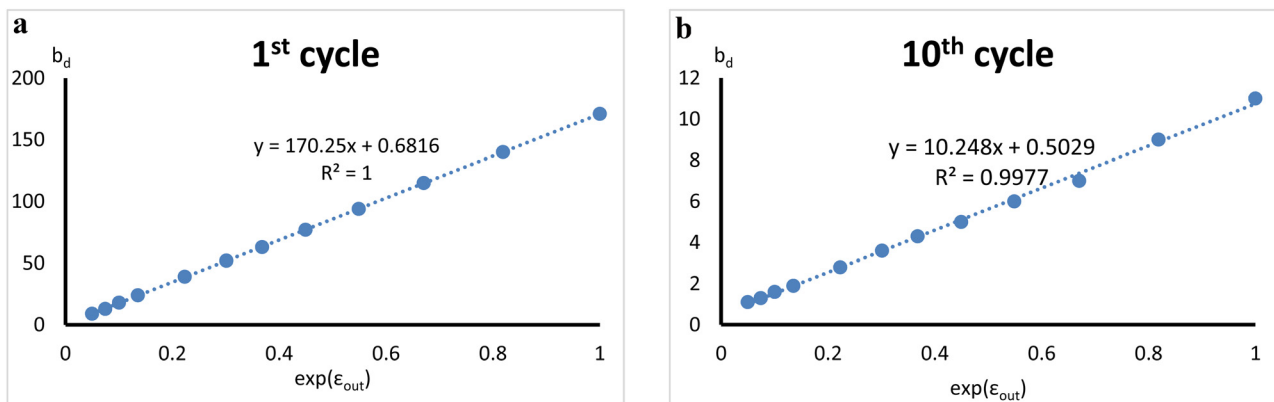


Fig. 9 (a) The relationship between upper limit of adsorption Na  $b_d$  and energy in the outer state  $\epsilon_{out}$  in the 1st cycle. (b) The relationship between upper limit of adsorption Na  $b_d$  and energy in the outer state  $\epsilon_{out}$  in the 10th cycle.

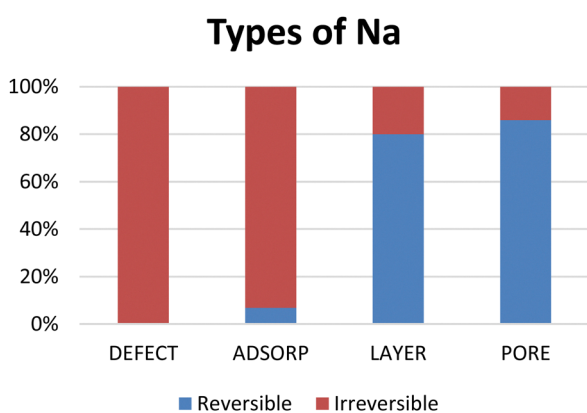


Fig. 10 Degree of reversibility and irreversibility of each type of Na in HC.

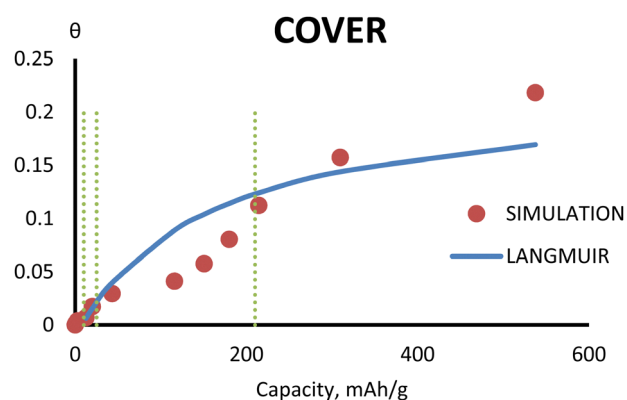


Fig. 11 The cover of the 1st cycle obtained from Langmuir theory (blue line) and simulation (red dots).

Inter pore Na capacity is due to the larger mobility of inter pore Na compared to interlayer Na.

These results are consistent with DFT calculations,<sup>40</sup> where the inter pore Na has the highest reversibility, while the average

irreversibility of other types is about 80%. However, our effective model helps to clarify the relative contributions of Na on defect sites, and Na adsorbed to graphitic layers to the capacity.



### 3.5 Comparison with Langmuir theory

The comparison between simulation and Langmuir theory<sup>53</sup> of the 1st cycle is shown in Fig. 11. Initially, Na adsorbs quickly on defect points. After that, the adsorbed Na follows the Langmuir theory. When Na starts to intercalate between graphitic layers, the amount of adsorbed Na decreases due to the interchange between adsorption Na and interlayer Na. When the interlayer sites for Na are saturated and the Na starts to fill the pore, the adsorbed Na follows Langmuir theory again. At very high capacity, the number of adsorbed Na ions is much higher than in the Langmuir theory.

## 4. Conclusions

To the best of our knowledge, we present the first effective model for Na insertion in the hard carbon anode, which comprises all known insertion mechanisms. Using specific material properties, combined with volume expansion and previous DFT calculations from the literature, we create an effective model with non – aligned graphitic domains and all possible energetically different insertion sites in the disordered structure. Our results agree with experiments for the OCV by taking into account the different mechanisms of Na insertion and the transitions between different insertion sites of Na. Also, the increase of irreversible capacity is captured within our model.

By comparing insertion for different cycles, a complete understanding of the capacity loss is gained. In the 1st cycle, four different insertion sites are accessible. Na atoms adsorb first on defect points  $O_C$  until the capacity  $C = 10 \text{ mA h g}^{-1}$  is reached. Then, Na will adsorb to the graphitic layers adjacent to pores. For capacities larger than  $C = 25 \text{ mA h g}^{-1}$ , Na atoms continue to adsorb to graphitic layers but some of the adsorbed Na interchange to the type interlayer Na until the interlayer structure  $NaC_{15.3}$  is formed at capacity  $C = 250 \text{ mA h g}^{-1}$ . Finally, Na can only fill the pore at a higher capacity. There are no Na atoms adsorbing on defect points  $2O_C$ , which means that  $2O_C$  defects prevent Na insertion in HC. The OCV results of the 10th cycle show similar behaviour to that of the 1st cycle, but there is no insertion to defect sites in 10th cycle anymore, since all sites remain occupied.

By comparing the 1st and 10th cycles, we can approximate the degree of reversibility of each type of Na in HC. The defect Na is irreversible due to the very strong interaction between Na and defect points. The fraction of reversibly adsorbed Na is also low because of the strong interaction between Na and graphite layers, while the proportion of reversible interlayer Na is high because of the weak interaction between Na and graphitic layers. This is clarified using DFT calculations:<sup>40</sup> only defect Na and adsorption Na are irreversible, while interlayer Na is highly mobile. Interpore Na is nearly reversible because the pore is large, compared with Na size, which means that they can move freely without restriction.

In future work, our model can be further developed to study transport properties as well as the diffusion pathway of  $Na^+$

from the cathode/electrolyte to HCs by using kinetic Monte Carlo simulation (KMC). The model can also be extended by combining many unit cells of HCs with different directions to describe the random structure of HCs.

## Author contributions

Huy Sy Nguyen contributed to conceptualization, data curation, formal analysis, investigation, methodology, designing computer program and writing original draft. Arnulf Latz contributed to project administration, supervision, validation, visualization, and writing – review and editing.

## Conflicts of interest

There are no conflicts to declare.

## Acknowledgements

This work contributes to the research performed at CELEST (Center for Electrochemical Energy Storage Ulm – Karlsruhe) and was funded by German Research Foundation (DFG) under project ID 390874152 (POLiS Cluster of Excellence). This study was also supported by computer resources from the University of Ulm and German Aerospace Center (DLR).

## References

- 1 A. Belgibayeva, A. Rakhmetova, M. Rakhmatkyzy, M. Kairova, I. Mukushev, N. Issatayev, G. Kalimuldina, A. Nurpeissova, Y. K. Soon and Z. Bakenov, *J. Power Sources*, 2023, **15**, 232550.
- 2 Y. Qiao, H. Zhao, Y. Shen, L. Li, Z. Rao, G. Shao and Y. Lei, *EcoMat*, 2023, e12321, DOI: [10.1002/eom2.12321](https://doi.org/10.1002/eom2.12321).
- 3 S. Özcan and B. Biel, *J. Appl. Phys.*, 2023, **133**, 044301, DOI: [10.1063/5.0131621](https://doi.org/10.1063/5.0131621).
- 4 W. Zou, A. Innocenti, M. Zarrabeitia, D. Bresser, Y. Yang and S. Passerini, *Acc. Chem. Res.*, 2023, **56**(3), 284–296, DOI: [10.1021/acs.accounts.2c00690](https://doi.org/10.1021/acs.accounts.2c00690).
- 5 K. Askaruly, M. Yeleuov, A. Taurbekov, B. Sarsembayeva, A. Tolyzbekov, N. Zhylybayeva, S. Azat, A. Abdisattar and C. Daulbayev, *Mater. Today Commun.*, 2023, **34**, 105136.
- 6 B. S. Lee, S. H. Oh, Y. J. Choi, M. J. Yi, S. H. Kim, S. Y. Kim, Y. E. Sung, S. Y. Shin, Y. Lee and S. H. Yu, *Nat. Commun.*, 2023, **14**, 150.
- 7 Y. Lai, X. Zhu, J. Li, Q. Guo, M. Li, A. Xia, Y. Huang, X. Zhu and Q. Liao, *Chem. Eng. J.*, 2023, **457**, 141196.
- 8 B. Biber, S. Sander, J. Martin, M. W. Mehrens and M. Mancini, *Carbon*, 2023, **201**, 847–855.
- 9 B. Heidrich, M. Stamm, O. Fromm, J. Kauling, M. Börner, M. Winter and P. Niehoff, *J. Electrochem. Soc.*, 2023, **170**, 010530.
- 10 A. F. Cuesta, S. A. M. Dickson, A. B. Naden, C. Longdale and J. T. S. Irvine, *J. Phys. Energy*, 2023, **5**, 015004.





- 11 A. V. Desai, V. R. Seymour, R. Ettlinger, A. Pramanik, A. S. Manche, D. N. Rainer, P. S. Wheatley, J. M. Griffin, R. E. Morris and A. R. Armstrong, *Chem. Commun.*, 2023, **59**, 1321–1324.
- 12 D. Kong, M. Tang, X. Wang, Z. Yuan and Y. Wang, *Appl. Surf. Sci.*, 2023, **616**, 156468.
- 13 Z. Mansouri, A. A. Shami, A. Sibari, S. Lahbabi, A. E. Kenz, A. Benyoussef, A. E. Fatimi and O. Mounkachi, *Phys. Chem. Chem. Phys.*, 2023, **25**, 3160–3174.
- 14 C. Chen, S. Guo, S. Gao, W. Chen, E. Abduryim, Y. Kuai, G. Wu, X. Guan and P. Lu, *Colloids Surf., A*, 2023, **662**, 131037.
- 15 A. Vasileiadis, Y. Li, Y. Lu, Y. S. Hu and M. Wagemaker, *ACS Appl. Energy Mater.*, 2023, **6**(1), 127–140.
- 16 H. Darjari, L. Bottoni, H. R. Moazami, S. J. Rezvani, L. Balducci, L. Sbrascini, A. Staffolani, A. Tombesi and F. Nobili, *Mater. Today Sustainability*, 2023, **21**, 100313.
- 17 H. Zhu, D. Wu, G. Zhang, W. Xu, A. Wang and K. Sun, *J. Energy Storage*, 2023, **57**, 106172.
- 18 B. Feng, L. Xu, Z. Yu, G. Liu, Y. Liao, S. Chang and J. Hu, *Electrochem. Commun.*, 2023, **148**, 107439.
- 19 S. Cho, J. C. Hyun, S. Ha, Y. Choi, H. Seong, J. Choi, H. J. Jin and Y. S. Yoon, *Carbon Energy*, 2023, **5**, e288, DOI: [10.1002/cey2.288](https://doi.org/10.1002/cey2.288).
- 20 A. Jo, B. Lee, B. G. Kim, H. Lim, J. T. Han, S. Y. Jeong, J. Kim, S. H. Seo, H. J. Jeong, G. W. Lee, K. J. Baeg, B. Jeong and J. H. Park, *Carbon*, 2023, **5**, 549–560.
- 21 K. C. Wasalathilake, G. A. Ayoko and C. Yan, *Carbon*, 2018, **140**, 276–285.
- 22 E. Olsson, G. Chai, M. Dove and Q. Cai, *Nanoscale*, 2019, **11**, 5274–5284.
- 23 E. Olsson, G. Cottom and Q. Cai, *Small*, 2021, **17**(18), 2007652, DOI: [10.1002/smll.202007652](https://doi.org/10.1002/smll.202007652).
- 24 M. A. Reddy, M. Helen, A. Groß, M. Fichtner and H. Euchner, *ACS Energy Lett.*, 2018, **3**, 2851–2857.
- 25 H. Euchner, B. P. Vinayan, M. A. Reddy, M. Fichtner and A. Groß, *J. Mater. Chem. A*, 2020, **8**, 14205–14231.
- 26 C. Cai, Y. Chen, P. Hu, T. Zhu, X. Li, Q. Yu, L. Zhou, X. Yang and L. Mai, *Small*, 2022, **18**, 2105303, DOI: [10.1002/smll.202105303](https://doi.org/10.1002/smll.202105303).
- 27 Y. Youn, B. Gao, A. Kamiyama, K. Kubota, S. Komaba and Y. Tateyama, *npj Comput. Mater.*, 2021, **4**, 48, DOI: [10.1038/s41524-021-00515-7](https://doi.org/10.1038/s41524-021-00515-7).
- 28 M. C. Mercer, S. Affleck, E. M. Gavilán-Arriazu, A. A. Zülke, P. A. Maughan, S. Trivedi, M. Fichtner, A. R. Munnangi, E. P. M. Leiva and H. E. Hoster, *Chem. Phys. Chem.*, 2022, **23**, e202100748.
- 29 X. Chen, Y. Zheng, W. Liu, C. Zhang, S. Li and J. Li, *Nanoscale*, 2019, **11**, 22196–22205.
- 30 J. Zhang, Y. Huang, C. Chen and K. She, *Energy Fuels*, 2023, **37**(3), 2379–2386.
- 31 I. Jeon, D. Yang, D. Yadav, J. Seo, H. Zhang, L. Yin, H. S. Ahn and C. R. Cho, *Electrochim. Acta*, 2023, **439**, 141730.
- 32 D. Qin, L. Wang, X. Zheng, J. Sheng, F. Huang, G. Xu, M. Zhu and Z. Dai, *Energy Storage Mater.*, 2023, **54**, 498–507.
- 33 N. T. Aristote, Z. Song, W. Deng, H. Hou, G. Zou and X. Ji, *J. Power Sources*, 2023, **558**, 232517.
- 34 B. Zhang, C. M. Ghimbeu, C. Laberty, C. V. Guterl and J. M. Tarascon, *Adv. Energy Mater.*, 2016, **6**(1), 1501588.
- 35 E. Irisarri, A. Ponrough and M. R. Palacin, *J. Electrochem. Soc.*, 2015, **162**(14), A2476–A2482.
- 36 L. Yang, M. Hu, H. Zhang, W. Yang and R. Lv, *J. Colloid Interface Sci.*, 2020, **566**, 257–264.
- 37 X. Chen, Y. Fang, H. Lu, H. Li, X. Feng, W. Chen, X. Ai, H. Yang and Y. Cao, *Small*, 2021, **17**(34), 2102248, DOI: [10.1002/smll.202102248](https://doi.org/10.1002/smll.202102248).
- 38 C. Bommier, W. Luo, W.-Y. Gao, A. Greaney, S. Ma and X. Ji, *Carbon*, 2014, **76**, 165–174.
- 39 D. Sauerteig, S. Ivanov, H. Reinshagen and A. Bund, *J. Power Sources*, 2017, **342**, 939–946.
- 40 A. C. S. Jensen, E. Olsson, H. Au, H. Alptekin, Z. Yang, S. Cottrell, K. Yokoyama, Q. Cai, M. M. Titirici and A. J. Drew, *J. Mater. Chem. A*, 2020, **8**, 743–749.
- 41 M. Schammer, B. Hortstmann and A. Latz, *J. Electrochem. Soc.*, 2021, **168**, 026511.
- 42 J. Lück and A. Latz, *Phys. Chem. Chem. Phys.*, 2018, **20**, 27804–27821.
- 43 L. von Kolzenberg, A. Latz and B. Horstmann, *ChemSusChem*, 2020, **13**, 3901–3910.
- 44 J. Newman and K. E. Thomas-Alyea, *Electrochemical System*, John Wiley & Sons, Inc., New Jersey, 2004.
- 45 J. Hao, Y. Wang, K. Sheng, Z. Tian, Y. Liu, W. Li and J. Li, *Fuel*, 2023, **332**(2), 126158.
- 46 L. Tao, P. Sittisomwong, B. Ma, A. Hu, D. Xia, S. Hwang, H. Huang, P. Bai and F. Lin, *Energy Storage Mater.*, 2023, **55**, 826–835.
- 47 F. Xie, Z. Xu, Z. Guo and M. M. Titirici, *Prog. Energy*, 2020, **2**, 042002.
- 48 H. S. Nguyen, J. Forsman and C. E. Woodward, *Soft Matter*, 2018, **14**, 6921–6928.
- 49 H. S. Nguyen, J. Forsman and C. E. Woodward, *J. Chem. Phys.*, 2019, **150**, 044906.
- 50 S. Qiu, L. Xiao, M. L. Sushko, K. S. Han, Y. Shao, M. Yan, X. Liang, L. Mai, J. Feng and Y. Cao, *Adv. Energy Mater.*, 2017, **7**, 1700403, DOI: [10.1002/aenm.201700403](https://doi.org/10.1002/aenm.201700403).
- 51 P. C. Tsai, S. C. Chung, S. K. Lin and A. Yamada, *J. Mater. Chem. A*, 2015, **3**, 9763–9768, DOI: [10.1039/C5TA01443C](https://doi.org/10.1039/C5TA01443C).
- 52 S. Alvin, D. Yoon, C. Chandra, H. S. Cahyadi, J. H. Park, W. Chang, K. Y. Chung and J. Kim, *Carbon*, 2019, **145**, 67–81, DOI: [10.1016/j.carbon.2018.12.112](https://doi.org/10.1016/j.carbon.2018.12.112).
- 53 O. Ziaee, N. Zolfaghari, M. Baghani and M. Baniassadi, *Phys. Scr.*, 2021, **96**, 125841.

